JOURNAL OF MATERIALS SCIENCE 13 (1978) 2403–2412

Hot pressing and physical properties of Na beta alumina

W. J. McDONOUGH, D. R. FLINN*, K. H. STERN, R. W. RICE
Naval Research Laboratory, Washington, DC 20375, USA

Dense transparent/translucent Na–β-alumina was hot pressed using commercial powders having low SiO_2 contents provided that agglomerates could be broken down by milling. Partial (up to 60 vol %) transformation to alpha alumina during hot pressing was caused by SiO_2 either present in some powders, or introduced by excessive milling or present through the addition of Na_2O–SiO_2 glass. Such transformation also results from increased storage time or from direct water contamination. Two wt % MgO was used to aid densification, and 2 wt % Na_2O to aid conductivity. Flexure strengths averaging 290 MN m^{-2}, a measured Young's modulus of 21.3×10^4 MN m^{-2}, and the observed pores or flaws at the fracture origins gave calculated values for the fracture energy in good agreement with the directly measured value of 13 J m^{-2}, for larger pores and flaws. The ionic resistivity was low, e.g. $\sim 3\,\Omega$ cm at 350° C. Effects of surface finish, limited porosity and hot pressing texture varied resistivity by up to a factor of 10.

1. Introduction

Beta aluminas, especially those containing sodium, are of interest for energy storage devices, e.g. the sodium–sulphur battery [1–4]. However, very dense materials, i.e. <1% porosity to minimize porosity effects in studying conductivity and chemical stability, have generally not been available. Improved sintering, e.g. zone sintering of Na–β-Al_2O_3 with 2 wt % MgO by Wynn Jones *et al.* [5] have ~0% open porosity, but a few % closed porosity. Further, both porosity and larger grain sizes in previous materials have often been a major factor in the lower mechanical strength of these materials, limiting their ability to withstand the thermal stresses, vibration and shock that will be important in many applications. For example, strengths of β-Al_2O_3 sintered by Francis *et al.* [6], from the same powder as in this study, were limited to 120 MPa by the ~3% porosity and >100 μm tabular grain size. Similarly, the strengths of the bodies used by Kennedy and Sammells [7] sintered from the same powder with MgO and Na_2CO_3 additives would have been presumably limited by their 7% porosity, had they been measured. Thus, McGeehin and Hooper's [8] recent review indicated that very dense Na–β-Al_2O_3 was still not available, but referenced preliminary work by the present authors as developing such dense bodies [9].

This paper reports the development of hot pressing techniques to produce dense, nearly transparent Na–β-alumina bodies from powders representative of commercial production. These bodies are characterized and the mechanical properties, which previously had not been thoroughly studied, are documented, especially those pertinent to strength and fracture. Ionic conductivity was also determined to show the utility of the resultant bodies. Some parameters influencing conductivity are discussed.

2. Experimental techniques

Calcined Na–β-Al_2O_3 powders† contained 7.3 wt % Na_2O (2% over stoichiometry), which were in pilot plant production and hence representative of commercial material, were used. Powder analysis by X-ray diffraction, spark source spectroscopy, and SEM in this programme (Table I) were similar

*Presently at the Bureau of Mines, College Park, Maryland.
†Powder from 4 lots, ALCOA Corp., East St Louis, Illinois.

to that of the other investigators [6, 7] characterizing powders from this same source. In all cases, X-ray analysis showed the powder to be of the β-form despite the excess Na_2O content. Powders were ball milled in porcelain jars with high Al_2O_3 balls under both wet and dry conditions (Table I), and with and without various certified purity additives.

Resultant milled powders were uniaxially hot pressed in graphite dies between 1500 and 1600° C with 5000 lb in^{-2} pressure for times ranging from 10 to 60 minutes. Initial selection of parameters was guided by the sintering and annealing studies of Francis *et al.* [6] and Kennedy and Sammells [7] using the same source of powder (as discussed later). Thus, temperatures were kept down to limit loss of Na_2O (0.2 wt % at 1500° C and 2.0 wt % at 1600° C on annealing [6]). The use of additional (up to 2 wt %) Na_2O and additions of MgO were also utilized to suppress Na_2O loss [7].

Dense cubes and slabs were cut from hot pressed discs and cylinders for density, X-ray analysis, ionic conductivity, i.r. transmission, and dynamic pulse-echo Young's modulus measurements [10]. The degree of crystallographic texturing relative to the hot pressing direction was determined by an inverse pole figure technique [11]. The large planar area of slabs for conductivity measurements was parallel to the hot pressing direction. Ionic conductivity was measured in our laboratory and three independent laboratories* using two methods. The first method, using a 2-probe sodium–electrolyte–sodium cell [9, 12, 13] measured 0.5 cm thick slabs from ~100° C to 450° C, at 10^2, 10^3, and 10^4 Hz a.c. and at d.c. current densities between 3 and 11 mA cm^{-2}. The second method, a 4-probe d.c. test cell, measured 2.5 cm cubes at 35° C with solid Na wafers lightly pressed onto the cubes faces [12].

Bars, cut with their axis parallel to and perpendicular to the hot pressing direction, and diamond ground parallel to their length with edges rounded, were used in 3-point flexure and thermal expansion tests. Fractured specimens were examined optically to determine grain size and fracture origins; more detailed fracture analysis was done by SEM. Critical fracture energies were measured with crack propagation on a plane parallel to the hot pressing direction using a double-cantilever-beam technique [14].

3. Results and discussion

Hot pressing performed as outlined above, often yielded bodies with ~0% porosity, fine (5 μm) grain size, high strength (280 to 350 MPa), and low resistivity (~3.0 ohm cm) at 350° C. In all cases, X-ray analysis showed only the Na–β-Al_2O_3 phase in the resultant bodies whether or not additives were used. However, some powder and processing conditions led to varying amounts of α-Al_2O_3. These conditions and other major processing observations are presented below followed by more detailed results of characterization and property evaluation.

3.1. Processing

Data for powder from the initial lot (A), which hot pressed without additives to a transparent/translucent 99+ relative density with good flexure strength, are shown in Table I. This lot, which was in limited supply, showed a progressive ageing of the powders, such that with increasing storage of the powder, even in sealed jars, increasing amounts of α-alumina occurred in the resultant hot pressed bodies. Data for other lots, which exhibited different results are also shown in Table I. For example, Lot B, which was superground by the supplier and found (by emission spectroscopy) to have 10-fold higher Si content (presumably as SiO_2) than Lot A, exhibited poor final density and partial transformation to α-Al_2O_3, so further work on this lot ceased. Lot C, which contained tough agglomerates, failed to give high densities before or after milling. Even 75 hours wet milling failed to break up the agglomerates. However, long milling times increased the SiO_2 content from the mills, e.g., even 100 hours of dry milling increased the SiO_2 content 15-fold. The hot pressed body contained 10–15 vol % α-alumina and, hence, work on Lot C was discontinued. Lot D contained dark coloured, iron-rich particles, "specks"; the majority of which were removed by hand after a magnetic separation removed ~10%. Trial hot pressings with Lot D (with specks removed unless noted otherwise) encouraged continued development.

Further trials plus the previous work showed three major guides to fabrication; First, the higher Si (i.e. SiO_2) content of both Lot B as received and Lot C (after extended milling) suggested using only lots with low SiO_2 contents and whose

*W. Fielder, NASA Lewis, Cleveland, Ohio; Toshiba Research and Development Center, Japan; and TRW, Redondo Beach, California.

TABLE I Powder analysis and summary of processing results

Starting powders			Milling results			Hot pressing results		
Lot no.	Summary impurity analysis (wt%)	Particle character	Medium	Time (h)	Resultant particle character	Density (% of theoretical)	Modulus of rupture (MPa)	Extra phases (%)
A	Si, 0.3 Mg, 0.3	20% (A)*	dry	70	(A) Broken up	99 +	295	none
A	Ca, 0.03	(P)† ≈ 100 μm	isopropanol	100	(P) ≈ 0.2 μm	100	–	33 α-Al_2O_3
B	Si, 2.5	5 to 10% (A)	as-received	–	5 to 10% (A)	96	175	trace α
B	Mg, 0.004	(P) ≈ 0.5 μm to	dry	5	(P) ≈ 0.5 μm	98	–	15 α-Al_2O_3
B	Ca, 0.003	(P) ≈ 5 μm	isopropanol	75	(p) ≈ 0.1 μm	100	–	60 α-Al_2O_3
C	Si, 0.4	30% (A)	dry	70	5 to 10% (A)	90	145	15 α-Al_2O_3
C	Mg, 0.02 Ca, 0.004	(P) ≈ 100 μm	isopropanol	75	(P) ≈0.5 μm	100	–	40 α-Al_2O_3
D	Si, 0.4	5 to 10% (A)	dry	1.0	trace % (A)	97	225	none
D	Mg, 0.003	(P) ≈ 100 μm	isopropanol	4.0	(P) ≈ 0.2 μm	96	222	none
D + MgO‡	Ca, 0.03		dry	1.0		99+	350	none

*(A) = agglomerates with 5 or more particles partially fused together.
†(P) = average particle size estimated from SEM.
‡2 wt % MgO.

agglomerate structure could be broken up with limited milling (to minimize SiO_2 from milling). The need for low SiO_2 content was corroborated by other experiments in which 10 wt % of sodium conducting glass ($Na_2O \cdot 3SiO_2$) powder was added to Lot D powder in order to give a sodium conducting body of high formability, e.g. to aid hot pressing of tubes. About 30 vol % of the Na–β-alumina was converted to α-alumina despite the 200° C lower hot pressing temperature (~1350° C), indicating SiO_2 can induce the β to α conversion. This enhanced α conversion by SiO_2 has been reported in other investigations [15, 16], and Lazennec [17] has subsequently reported enhanced β to α conversion due to SiO_2 and sodium silicate. Investigation of milling parameters to maximize agglomerate break-up in limited milling times showed dry milling to be better than wet for Lot D. Therefore, Lot D powders freshly dry milled for one hour gave hot pressed bodies ⩾98% of theoretical density with strengths about equal to those from Lot A.

The second processing guide found was that powders should be used soon after milling as indicated by earlier noted ageing of Lot A (and some in Lot D), even though stored to minimize moisture pick-up. While X-ray analysis of powders stored for longer periods of time still showed only the β-phase, powders stored for 2 days in water exhibited ~10% β to α conversion as well as dendritic crystals identified as hydrated Na_2CO_3. Hot pressing of the previously water soaked powders, from which water was removed only by drying, resulted in a 2- to 3-fold increase in the resultant α-alumina indicating enhanced β to α conversion during hot pressing of powders exposed to H_2O (note the $NaCO_3$ and resultant Na_2O content cannot be responsible for the conversion since its addition does not cause conversion as discussed below).

The third processing guide found was that the higher MgO content of Lot A (Table I) and its good densification suggested the use of an MgO addition to Lot D which had lower MgO content, as did Lots B and C. Such usage of MgO is also known to be advantageous in inhibiting α conversion and giving lower resistivities [7]. Also, to compensate for possible Na loss during hot pressing, 2 wt % Na_2O was added in the form of Na_2CO_3. Such combined MgO–Na_2O additions to Lot D followed by 1 hour dry milling repeatedly resulted in transparent/translucent, single phase hot pressed Na–β-alumina. Thus, unless noted otherwise, further results are for bodies made by such processing of Lot D powder. Limited trials with additions of either 2 wt % NaF or LiF dry milled with Lot D powders (but with no other additives), were also made in an attempt to lower hot pressing temperatures, and possibly aid formability. This did give 99 + % relative density at hot pressing temperatures

of 1350° C, i.e. 250 to 300° C lower than without these additives. However, such bodies give poor ionic conductivities, as briefly discussed later.

3.2. Characterization

Bodies with about 1% or more porosity were a homogeneous opaque white colour. As lower porosity was achieved, translucent lens-shaped laminar regions formed indicating inhomogeneous final densification common to many hot pressed materials, e.g. α-alumina [18]. Further reduction in porosity (to <1%) gave homogeneous transparent/translucent light grey bodies (Fig. 1). The grains were equiaxed, commonly averaging about 5 μm, and showed no tendency for development of the large tabular grains typically found in the bimodal grain structures of sintered Na–β-aluminas [19]. Porosity was almost, if not exclusively, intergranular. As noted earlier, previous sintering of powders from the same source gave minimum porosity of ~3% and a grain size >100 μm (tabular) without additives [6], and a porosity of 7% with similar Na_2O and MgO additives [7] as used in this study.

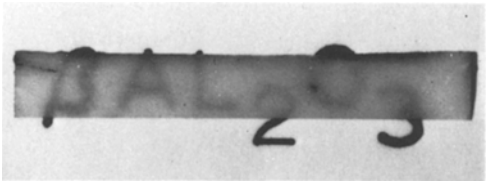

Figure 1 Translucent/transparent Na–beta alumina hot-pressed 5000 lb in^{-2}, 1525° C, 30 min in air. Section is ~30 μm thick, diamond saw-cut only.

X-ray analysis showed that, except for some α-Al_2O_3 in cases noted earlier, only the β form of Na_2O–Al_2O_3 was present, which is consistent with the sintering results of Francis *et al.* and Kennedy and Sammells using powder from the same source, without and with similar additives of this study, respectively. X-ray analysis, however, did reveal some texturing from hot pressing as shown by the inverse pole figure which compares X-ray intensities of prominent lines in a powder sample (i.e. random grains) to the textured body (Fig. 2). An "*R*" value for a given diffracting plane was obtained by comparing its normalized intensity from a textured, in this case a hot pressed sample, to its normalized intensity for a truly random crystallographic orientation, i.e. $R = 1$ for a random crystallographic orientation. Thus, *R* values on hot pressed Na–β-alumina were ~2 to 3 for both the face parallel to and perpendicular to the hot pressing direction, indicating a [1 1 0] texture and a [0 0 1] basal texture, respectively. Forged alpha alumina [20] shows similar basal [0 0 1] texture perpendicular to the hot pressing/forging direction with *R* values (between 2 and 15) increasing with the amount of deformation.

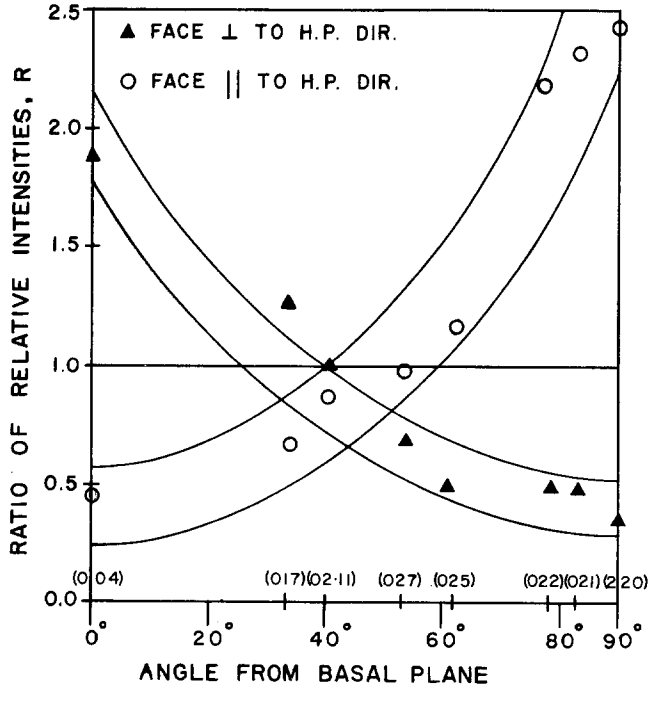

Figure 2 Inverse pole figure showing slight degrees of texturing on faces both perpendicular to and parallel to the hot pressing direction. (Average of four hot pressings.)

TABLE II Summary of physical property measurements on Na-β-alumina

Property	Measurement	
Density	3.26 g cm^{-2} (by Archimedes method)	
MOR	290 ± 40 MN m^{-2} (35 specimens) 3 pt., 0.12 cm min^{-1}	
Critical fracture energy	13 ± 3 J m^{-2}	
Grain size	1 to 5 μm equi-axed	
Hardness	1300 to 1524 H_v 14 samples at 200, 500, or 100 g loads	
Thermal expansion	20° C to 500° C, $\alpha = 7.00 \times 10^{-6}$ (° C)$^{-1}$ 500° C to 1000° C, $\alpha = 8.03 \times 10^{-6}$ (° C)$^{-1}$ 1000° C to 1400° C, $\alpha = 9.48 \times 10^{-6}$ (° C)$^{-1}$	
*Youngs's modulus	21.3 × 10^4 MN m^{-2}	⊥ to HP† direction
	19.3 × 10^4 MN m^{-2}	∥ to HP direction
*Poisson's ratio	0.27	⊥ to HP direction
	0.26	∥ to HP direction
*Bulk modulus	15.4 × 10^4 MN m^{-2}	⊥ to HP direction
	15.0 × 10^4 MN m^{-2}	∥ to HP direction
i.r transmission	Transmission from 3.5 μm to ~6.0 μm peaking about 15% transmission between 4.5 μm and 5.5 μm.	
Ionic resistivity	3.0 Ω cm at 350° C	Activation energy, 6.0 k cal mol^{-1} in direction perpendicular to uniaxial hot pressing direction.
	300 Ω cm at 35° C	

*Error in measurements calculated to be between 0.1 and 0.4%.
†Hot pressing.

A transparent/translucent specimen, ~0.025 in thick with ground surfaces, gave i.r. transmission from 3.5 μm to ~6.0 μm peaking at 15% transmission between 4.5 μm and 5 μm. The thermal expansion coefficient measured normal to the hot pressing direction from 20° C to 1400° C was 10 to 15% smaller than the values reported for alpha alumina (see Table II).

3.3. Mechanical properties

Results from strength, fracture energy, hardness, and elastic measurements are given in Table II. The latter, measured by a pulse echo technique, showed Young's modulus to be about half that of α-Al_2O_3, and revealed about 10% anisotropy due to the hot pressing texture. The value of Young's modulus in this study (~21 × 10^4 MPa) agrees well with that reported by Virkar and Gordon [21] for dense Li stabilized Na–β-Al_2O_3 and with the value quoted by Tan and May [22]. Steven's [23] value (16 × 10^4 MPa) for dense, hot pressed Na–β-Al_2O_3 is substantially lower.

No effect of the crystallographic texture could be observed on strength, e.g. a set of 35 Lot D specimens (specks removed) averaged 290 ± 40 MPa regardless of bar orientation relative to the hot pressing direction. It may be noted that when most of the specks were not removed from Lot D, strengths were about 20% lower. (Further analysis is based only on material with specks removed.) Thus, the resultant processing of this study yields flexural strengths of 280 to 350 MPa. These compare with upper limits of strengths of 330 MPa for Steven's hot pressed bodies, 200 MPa for Virkar and Gordon's sintered bodies (Li_2O stabilized Na–β-Al_2O_3) and Tan and May's sintered Na–β-Al_2O_3 (also Li_2O stabilized).

Examination of fractures from Lot D and earlier lots showed total transgranular failure (Figs. 3 and 4). A significant fraction, i.e. up to 70%, of all fracture origins occurred from large isolated pores (30 to 70 μm in diameter), generally located inside the sample rather than on the tensile surface, especially in the weaker samples (Fig. 3). Machining flaws, most commonly approximated as penny-shaped (Fig. 4), were also clearly observed where such flaws were larger and hence more readily observed.

The strength and fracture energy measurements were compared with the fractographic results by calculating the fracture energy (γ) for each failure using $E = 21 \times 10^4$ MPa, the observed flaw size, a, and the equation [24]

$$\gamma = Z\sigma^2 a/E \quad (1)$$

where σ is the fracture stress and Z is a flaw shape factor ranging from 0.8 for a surface half penny crack to 1.96 for a surface slit crack and from 0.64 for an internal penny-shaped flaw (pore) to 1.57 for a highly elongated elliptical flaw (pore). For

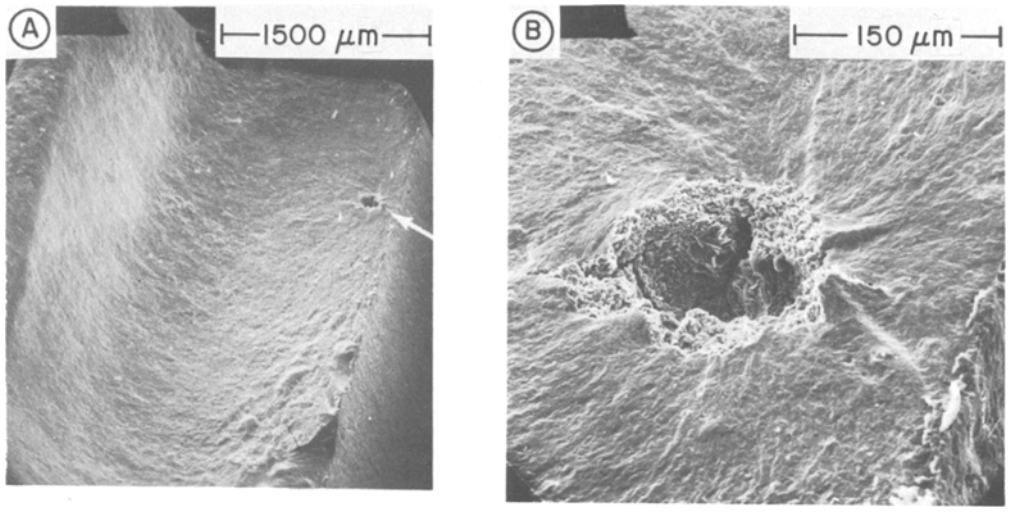

Figure 3 Fracture origin from a large pore; (A) low magnification of fracture, note large (120 μm) pore (arrow) at origin near the tensile surface; (B) High magnification of pore at origin, note transgranular fracture and associated fracture steps radiating from the pore showing it is the fracture origin. Using the pore size plus the grain size of ~5 μm, the measured flexure strength = 270 MPa and Young's modulus gives a fracture energy of 15.5 J m^{-2}.

machining flaws, the flaw size, a, was the flaw depth, while for pores the flaw size was taken as the pore radius plus the grain size (G) [25]. Only for smaller pores did the addition of G make a measurable difference. For eight specimens clearly failing from surface flaws, $\gamma = 12.1 \pm 2.4$ J m^{-2} in good agreement with the directly measured value of $\gamma = 13$ J m^{-2}. It was, however, observed that smaller flaws gave the lower values of fracture energy.

Calculations for specimen pore origins gave fracture energies increasing with pore size, then levelling off at ~13 J m^{-2} similar to the behaviour and values for machining flaws. The lower average fracture energies calculated from such origins resulted from the fact that pore origins could be clearly determined to smaller sizes than could machining flaws. The agreement between fracture energy calculated using the "pore size plus the grain size as the flaw" and similar sized surface

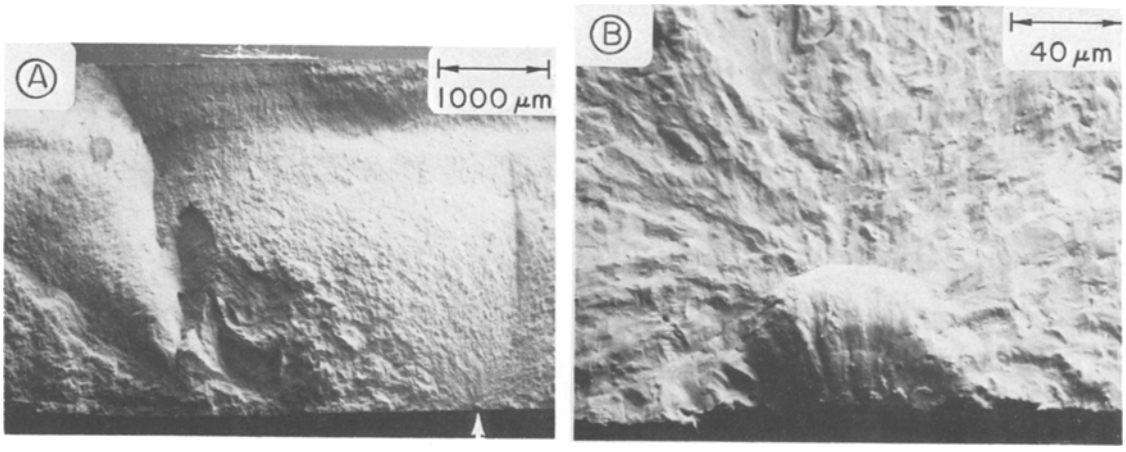

Figure 4 Failure from a machining flaw; (A) low magnification photo of fracture surface, note origin from flaw (arrow) surrounded by mirror, mist and hackle (especially on left because of location of origin nearer to the right-hand edge of the sample); (B) higher magnification of flaw at origin, note approximate penny shape (depth ~60 μm) of flaw, transgranular failure and radiating fracture steps. Using the measured flexure strength of 35 400 lb in^{-2} the flaw size and Young's modulus, a fracture energy of 13.8 J m^{-2} was calculated.

TABLE III Liquid Na cell two-probe resistivities (R)* on polycrystalline Na–β-Al_2O_3 with 2 wt % MgO and 2 wt % Na_2O

Sample description			Temperature range (° C)	Activated energy (kcal mol^{-1})	2-probe R (Ω cm)	
Sample type	Surface finish	Porosity (%)			350° C	35° C
Surface finish and porosity dependence†						
H5-81 Slab A	1 μm diamond finish	< 0.05	100 to 350 200 to 350	6.0 7.0	3.12[a] 2.93[b]	294‡ 478
H5-81 Slab B	350 mesh sawcut	< 0.05	200 to 350	7.0	7.50[b]	1300‡
H5-83 Slab B	350 mesh sawcut	0.05 to 0.10	100 to 300	6.0	12.4[d]	1040‡
H5-82 Slab A	350 mesh sawcut	0.30 to 0.80	100 to 300	6.2	21.2‡[d]	1550‡
H5-82 Slab B	350 mesh sawcut	0.30 to	35 to 300	6.2	54‡[a]	4350
Hot pressing orientation dependence						
H5-83† Slab A	350 mesh sawcut	0.05 to 0.10	150 to 450	4.0	8.6[c]	170‡
H5-83§ Slab A	350 mesh sawcut	0.05 to 0.10	150 to 450	4.6	19.6[c]	445‡

*NASA Lewis large single crystal measured between 100 and 315° C extrapolated to 3.52 cm at 350° C and 100 Ω cm at 35° C for 3.7 kcal mol^{-1} activation energy, 4-probe measurements give single crystal values of 4056 Ω cm at 350° C [12].
†Measured perpendicular to hot pressing direction.
‡Measured parallel to hot pressing direction.
§Extrapolated from test temperature range.
[a]NASA Lewis; [b]NRL; [c]Toshiba R and D Center; [d]TRW R and D Center measurements.

flaws corroborates such treatment of failure from pores. The decrease in fracture energy calculated with decreasing pore size is attributed to internal stresses from thermal expansion anisotropy [26], similar to effects seen in $BaTiO_3$ [27].

The authors' value of fracture energy is reasonably consistent with that recently reported by Virkar and Gordon [21] for similar grain sizes (i.e. ~14 and ~20 J m^{-2}, respectively) for crack propagation on a plane parallel and perpendicular to the hot pressing direction. Tan and May [22] report fracture energies of ~25 J m^{-2} calculated from flaw sizes. However, May agrees that use of $\sigma_f = 1.25\sqrt{(EV/C)}$ would have been more appropriate to make this calculation than $\sigma_f = 0.8\sqrt{(EV/C)}$ which they used [28]. This correction reduces their calculated fracture energy to ~10 J m^{-2} in good agreement with present results. Tan and May's somewhat lower corrected value relative to that of this study is reasonable in view of the expected lowering of γ due to their 1 to 3% porosity. (Note that their smaller flaw sizes are similar to the larger flaw sizes in this study, so no effects of internal stresses are expected.) This leaves only Stevens [23] reporting such a high, ~26 J m^{-2} fracture energy. However, his higher value may be due to microcracking found in detailed microscopy. Microcracking would also explain Steven's lower Young's modulus study and his somewhat lower average strengths, 300 MPa, despite a smaller average (~2 μm) grain size. Note that Stevens made an error in calculating flaw sizes; his data implies a flaw size of ~60, not ~25 μm. However, his suggestion that larger grains (to at least 10 μm, and possibly twice this value) may be the source of failure may be valid, recognizing that flaws in them would be controlled by fracture energies at or closer to those for preferred single crystal cleavage instead of polycrystalline values.

3.4. Ionic conductivity

The most significant resistivity result is that dense Na–β-alumina bodies, hot pressed from commercial

powders with 2 wt% each of MgO and Na_2O, had low resistivities. Typical resistivity values from dense translucent/transparent polished specimens were 3 to 5 Ω cm at 350° C (2-probe measurements) (see Table III). These measurements were duplicated by two other laboratories [12, 13] using their own sodium–electrolyte–sodium cells on the same specimens. All three results as a function of temperature gave activation energies of $\sim 6\,kcal\,mol^{-1}$ and fitted one straight line on a resistivity versus $1/T$ plot independent of frequency. The original purpose of the MgO addition was as a sintering aid to the Na–β-alumina but it appears to have lowered the polycrystalline resistivity to values normally reported for Na–β″-alumina [21], though no β″-phase was detected. However, limited quantities of β″-phase could be along grain boundaries, aiding conductivity, but not detectable by X-ray methods.

Resistivity values of 3.0 Ω cm at 350° C (3.6 Ω cm at 300° C) from this study can be compared with Virkar and Gordon's [21] Li_2O stabilized Na–β″-alumina values of ~5 Ω cm at 300° C with a tabular grain size of ⩽300 to 400 μm. Similarly, Whalen *et al.* [29] reported values as low as 5 Ω cm at 300° C for Na–β″-alumina with a bimolar grain distribution. Kennedy [30] reported values from various investigators for Na–β-alumina with additives ranging from 5 to 10 Ω cm at 300° C. The low resistivities of this study are consistent with Power's [31] observation that his minimum resistivities of 6 to 8 Ω cm at 300° C were obtained as a function of additive levels at 7.2 wt% Na_2O and 1 to 2 wt% MgO when sintering the same powders used in this study.

In addition to showing low resistivity, the resultant hot pressed bodies showed other effects. While there are variations in the electrical measurements by the various organizations, relative measurements within or between these organizations corroborate several partially understood or expected surface and microstructural results. Consider first surface effects. In the 2-probe tests, which are sensitive to surface effects, a high interfacial resistivity was always observed during initial heating up of the samples. This interfacial resistivity decreased as the temperature increased, disappearing at ~200° C for a polished slab and ~350° C for an as-sawn slab (350 mesh diamond blade); both slabs were cut side by side from the same specimen. This effect is atrributed to the expected surface films, e.g. Na_2CO_3 and NaOH, and is consistent with the limited solubility of such films increasing 4-fold between 200 and 350° C [32]. Since the rougher saw-cut surface would contain more film, i.e. from local deposits in machining striations and therefore more film per unit projected area, it would require higher temperatures for its removal, consistent with the observed behaviour. This initially higher resistivity is consistent with Armstrong's [33] observations in his metal–electrolyte–metal cell, and his suggestion of an initial unwetted interfacial impedance that gradually gives way to a "wetted" condition with time; longer times were required for a rougher surface. In our experiment, higher temperature apparently had the same effect as longer time, as expected.

After the above initial interfacial resistivity effect had disappeared there was still a significant effect from the surface finish. Thus 2-probe resistivitities, from slabs cut side by side from the same specimen, measured at 350° C were 3.0 Ω cm and 7.5 Ω cm, respectively, for samples with a 1 μm polished surface and an as-sawn surface. Armstrong also observed similar surface finish effects which he attributed to decreasing surface roughness as finer surface finishes were obtained. However, it is suggested that other machining effects besides roughness could play an important and possibly dominant role. Machining studies [34] clearly show that: (a) sawing produces a much greater depth of work hardening and larger flaws than polishing and hence greater potential for ion blockage due to the increased depth of disorder or irregularity of conduction paths near the surface and (b) temperatures localized at the saw blade–ceramic interface could be high enough to cause some phase transformation with the transformed α-alumina blocking the sodium ions. This suggests annealing or etching studies, provided they can be done without preferential loss of sodium.

Having sorted out the surface effects, several microstructural effects were then determined. The first microstructural result is the difference in resistivity resulting from the textural effects of hot pressing. Two bars cut from the same slab, one perpendicular to and the other parallel to the hot pressing direction, gave as-sawn resistivities of 8 Ω cm and 19 Ω cm at 350° C, respectively, despite the somewhat limited texture ($R = 2$ from the inverse pole plot). This texture effect can be readily understood by using simplified models considering conductivity as a series combination

of (a) grain boundary conduction and (b) bulk conduction of the single grains (crystals). Clearly texturing reduces the effective lengths of the grain boundary path in one set of directions and increases it in the other direction. Higher textures, e.g. $R \approx 15$ as reported for forged α-alumina [20], could give conductivity still closer to single crystal values perpendicular to the hot pressing or forging direction.

The second microstructural effect is the significant increase that even limited porosity, e.g. ~1%, had; increasing the resistivity ten-fold. While some investigators [35, 36] have indicated that porosity in Na–β-Al_2O_3 does not lower conductivity, others (e.g. Armstrong) have. It is suggested that these reported differences reflect primarily effects of pore location. Increased porosity must reduce the cross-sectional area for conductivity and hence increase the resisitivity. Grain boundary porosity should be the most detrimental because grain boundaries should commonly be a higher resistivity path to connect the conducting planes of highly misoriented adjacent grains, e.g. as indicated by the above texture effects. Hence comparable reductions in the conducting cross-sections of the higher resistivity boundaries should have significantly more effect than in the lower resistivity grains. Pore shape variations between different pore locations and different bodies may also be a factor.

In the present studies, variations in the amount of the primarily intergranular porosity resulted from minor changes in hot pressing time or temperature that produced essentially identical grain sizes and are unlikely to significantly change second phase distributions. In previous studies little or no characterization of porosity has been presented. However, sintered bodies, often with large tabular grains, were typically used. Thus greater amounts of intragranular porosity would typically be much more prevalent in many of these bodies.

Finally, measurements of samples made with fluoride additives showed these additives to be very detrimental. Specimens hot pressed with either 2 wt% LiF or NaF as the densification aid (instead of MgO) gave very large room temperature resistivites, 24 000 Ω cm and 30 000 Ω cm for 4-probe tests and twice these values for 2-probe tests as compared to 750 and 1500 Ω cm for two sets of bodies hot pressed with 2 wt% MgO having similar (1 to 2%) porosity. The fluoride additives appeared to inhibit the Na conductor and hence negated the beneficial fabrication effect of lowering the hot pressing temperature from 1600° C to 1350° C. Since such additivies are typically left at grain boundaries [37], this again supports the importance of the grain boundary character.

4. Summary and conclusions

This work showed that dense transparent/translucent equi-axed polycrystalline Na–β-alumina can be routinely hot pressed from commercial powders when appropriate attention is paid to impurities and agglomerates. Typical conditions were 1600° C, with 5000 lb in^{-2} for 60 min using graphite dies in a hot press open to the atmosphere. Addition of 2 wt% MgO aided densification and was effective in reducing resistivity, possibly due to forming a more conductive grain boundary phase like Na–β''-alumina. The resultant dense, hot pressed bodies had good ionic conductivity, e.g. resistivities of 3.0 Ω cm at 350° C, equal to single crystal Na–β-alumina. Measurable texturing resulted from hot pressing giving a significant, e.g. 2-fold, anisotropy in ionic resistivity, limited (10%) anisotropy in Young's modulus and no detectable anisotropy in flexural strength. The ~5 μm grain size specimens exhibited flexure strengths to 350 MPa and failed primarily from 40 to 50 μm sized pores and machining flaws consistent with measured fracture energies of 13 J m^{-2}. Consideration of grain orientation, porosity, and additive effects on ionic conductivity show that more attention to surface and microstructural, especially grain boundary, character is needed to fully understand conductivity behaviour.

Acknowledgement

The authors are grateful to Dr William L. Fielder of NASA Lewis for his stimulating discussion, to Dr Karl-Heinz Raffalski of Theta Industries for the thermal expansion measurements, and Dr Stephen W. Freiman of the US Naval Research Laboratory for fracture energy measurements.

References

1. M. S. WHITTINGHAM and R. A. HUGGINS, 'Proc. Solid State Chemistry,' edited by R. S. Roth and S. J. Schneider, Jr., (NBS Spec. Pub. 364, Washington, D. C. 1972) p. 139.
2. R. C. DEVRIES and W. L. ROTH, *J. Amer. Ceram. Soc.* **52** (1969) 364. 1969.
3. J. T. KUMMER, "Prog. Solid State Chem.", edited by H. Reiss and J. O. McCaldin, (Pergamon Press, New York, 1972) p. 141.

4. W. VANGOOL, "Annual Review Materials Science", Vol 4 (Annual Reviews Inc., Palo Alto, 1974) p. 311.
5. I. WYNN JONES and L. J. MILES, *Proc. Brit. Ceram. Soc.* **19** (1971) 161.
6. T. L. FRANCIS, F. E. PHELPS and G. MACZURA, *Amer. Ceram. Soc. Bull.*. **50** (1971) 615.
7. J. H. KENNEDY and A. F. SAMMELLS, *J. Electrochem. Soc.* **119** (1972) 1609.
8. P. McGEEHIN and A. HOOPER, *J. Mater. Sci.* **12** (1977).
9. D. R. FLINN, W. J. McDONOUGH, K. H. STERN and R. W. RICE, *Electrochem Soc. Ext. Abs.* **75** (1975) 23.
10. H. B. HUNTINGTON, *Phys. Rev.* **72** (1947) 321.
11. C. S. BARRETT and T. B. MASSALSKI, "Structure of Metals," (McGraw–Hill, New York, 1966).
12. W. L. FIELDER, S. FORDYCE and J. SINGER, NASA Report No. TMX-71546.
13. A. IMAI and M. HARATA, *Jap. J. Appl. Phys.* 8 (1972) 180.
14. S. W. FREIMAN, D. R. MULVILLE and P. W. MAST, *J. Mater. Sci.* 8 (1973) 1527.
15. M. SHAD, B. DUNN, M. MINAMI and J. D. MACKENZIE, presented at 77th Meeting, Amer. Ceram. Soc., Washington D. C. 1975.
16. F. Y. TSIANG, presented at 77th Meeting, Amer. Ceram. Soc., Washington D. C., 1975.
17. Y. LAZENNEC, private communication (1976).
18. R. W. RICE, NRL Report No. 7111, Naval Research Laboratory, Washington D. C., 1970.
19. R. W. POWERS and S. P. MITOFF, *J. Electrochem. Soc.* **122** (1975) 226.
20. W. H. RHODES, D. J. SELLERS and T. VASILOS, *J. Amer. Ceram. Soc.* **58** (1975) 31.
21. A. V. VIRKAR and R. S. GORDON, *ibid.* **60** (1977) 58.
22. S. R. TAN and G. J. MAY, *J. Mater. Sci.* **12** (1977) 1058.
23. R. STEVENS, *ibid.* 9 (1974) 934.
24. G. R. IRWIN and P. C. PARIS, "Fracture – An Advances Treatise", Vol III, edited by H. Liebowitz, (Academic Press, New York, 1971).
25. A. G. EVANS and R. W. DAVIDGE, *J. Nuclear Mater.* **33** (1969) 249.
26. R. W. RICE, R. C. POHANKA, and W. J. McDONOUGH, to be published.
27. R. C. POHANKA, R. W. RICE, B. E. WALKER and P. L. SMITH, *Ferroelectrics* **10** (1976) 231.
28. G. J. MAY and R. W. RICE, private communication (1977).
29. T. J. WHALEN, G. J. TENNENHOUSE and C. MEYER, *J. Amer. Ceram. Soc.* 57 (1974) 497.
30. J. H. KENNEDY, "Superionic Conductors", ed. G. D. Mahan and W. L. Roth, 351-68, (Plenum Press, New York, 1976) p. 351.
31. R. W. POWERS, *ibid.*, p. 351.
32. D. D. WILLIAMS, J. A. GRAND and R. R. MILLER, NRL Memorandum Report No. 424, Naval Research Laboratory, Washington D. C., 1955.
33. R. D. ARMSTRONG, T. DICKINSON and J. TUNRER, *Electroanalyt. Inter. Electrochem.* **44** (1973) 157.
34. R. W. RICE, Proceedings of the Second Army Materials Technology Conference, sponsored by Army Mtls. and Mech. Res. Center, Watertown, Mass., 1973.
35. G. J. TENNENHOUSE, R. C. KU, R. H. RICHMAN and T. J. WHALEN, *Amer. Ceram. Soc. Bull.* **54**, (1975) 923.
36. M. HARATA, private communication (1975).
37. W. C. JOHNSON, D. F. STEIN and R. W. RICE, *J. Amer. Ceram. Soc.* 57 (1974) 342.

Received 26 July 1977 and accepted 27 February 1978.